nature geoscience

ARTICLES

PUBLISHED ONLINE: 19 OCTOBER 2015 | DOI: 10.1038/NGEO2568

Southward shift of the northern tropical belt from 1945 to 1980

Stefan Brönnimann[1,2]★, Andreas M. Fischer[3], Eugene Rozanov[4,5], Paul Poli[6], Gilbert P. Compo[7,8] and Prashant D. Sardeshmukh[7,8]

Changes in the position and width of the tropical belt are societally and ecologically relevant, because they are associated with shifts of the subtropical dry zones. The tropical belt has widened since about 1980, but little is known about its earlier variability. Here we analyse historical surface and upper-level observations, three global reanalysis data sets, and a reconstruction of total column ozone, to show that the northern tropical edge retracted from 1945 to 1980, while the northern Hadley cell shifted southwards in both summer and winter. We present chemistry–climate model simulations that reproduce the retraction and southward shift. We find that retraction of the tropical belt was largely due to cooling sea-surface temperatures north of the Equator and warming south of the Equator, most prominently over the Atlantic. Substantial hydroclimatic anomalies such as European droughts of the 1940s and 1950s and the Sahel drought of the 1970s were associated with this shift of the Hadley cell. Our results suggest that multidecadal changes in the position of the northern Hadley cell are an important component of climate variability.

The tropical belt is the region influenced by the meridional atmospheric circulation cell known as the Hadley cell (illustrated by the zonal mean meridional mass stream function ψ in Fig. 1 for boreal winter). Its equatorward branch is marked by the Intertropical Convergence Zone (ITCZ), a region of high precipitation and associated strong ascent of moist air. It is also a zone with often calm surface winds over the oceans (equatorial calms). At its poleward branch, air masses descend and precipitation is accordingly low. The poleward edge of the tropics can be defined in zonally averaged meteorological fields by the positions of features (Fig. 1) such as another region of relatively calm surface winds over the ocean (subtropical calms), high sea-level pressure (subtropical highs), strong descent in the free troposphere, the subtropical jet at around 200 hPa, and the 'subtropical ozone front' (a steep ozone increase towards the midlatitudes that is related to the change in tropopause altitude)[1–3].

Recent tropical widening, unknown past

Since the edge of the tropical belt affects the position of the subtropical dry zones, decadal shifts or trends in the tropical edge such as the observed widening since about 1980 (refs 1–5) may determine the transition between drought and non-drought conditions and are therefore highly relevant for society. While droughts in Australia have been attributed to the current widening of the tropical belt[6], the relation of past decadal hydroclimatic changes to shifts in the tropical belt has received less attention. Here we focus on hydroclimatic changes over the period 1945–1980, as depicted in precipitation trends (Fig. 2; see Supplementary Fig. 1 for significance). Southern and Central Europe were affected by severe summer drought from about 1945 to the early 1950s, then precipitation increased. The Southern USA suffered from drought in the early 1950s while summers got wetter in the subsequent decades. Conversely, in the Sahel region pluvial conditions prevailed in the 1950s, followed by severe drought in the 1970s (a similar pattern is found in the Orinoco basin[7]). Previous work has linked the Sahel drying to a southward shift of the ITCZ (refs 8,9), but changes of the northern edge of the tropical belt and their relation to hydroclimatic anomalies have not been addressed.

As early as 1969, the eminent climatologist H. H. Lamb noted (among other climatic changes) an equatorward shift of the subpolar cyclones, subtropical anticyclones, and arid zones during the 1950s and 1960s based on sea-level pressure data[10]. In a recent paper, Allen *et al.*[11] report a contraction of the northern tropical belt from 1950 to 1979 in climate model simulations and observation-based data (Version 2 of the atmospheric reanalysis 20CR; ref. 12). However, they found that trends are weak and ambiguous, as are trends based on other reanalyses for the 1958–1979 period[13]. Further evidence is thus required.

A multi-evidence approach

Even regarding the widening of the tropical belt since 1979, magnitudes derived from reanalyses are uncertain[2,5,13,14] and confidence in the widening rests on the fact that it is evident in different, independent data sets and indicators (atmospheric reanalyses, outgoing long-wave radiation, total column ozone[5], among others). The availability of multiple data sets has restricted most research to the post-1979 era.

Recently, new data sets have been produced for earlier decades that allow a more robust view of changes in the tropical belt before 1979. In addition to sea-level pressure (HadSLP; ref. 15), marine surface winds (ICOADS, v2.5; ref. 16), and the surface-driven 20CR reanalysis Version 2, a new version of 20CR (Version 2c) and another long, surface-driven reanalysis data set, ERA-20C, have been released[17]. Furthermore, two reconstructions of upper-level

[1]Oeschger Centre for Climate Change Research, University of Bern, CH-3012 Bern, Switzerland. [2]Institute of Geography, University of Bern, CH-3012 Bern, Switzerland. [3]Federal Office of Meteorology and Climatology MeteoSwiss, CH-8058 Zurich, Switzerland. [4]Physical-Meteorological Observatory/World Radiation Center PMOD/WRC, CH-7260 Davos, Switzerland. [5]Institute for Atmospheric and Climate Sciences, ETH Zurich, CH-8092 Zurich, Switzerland. [6]European Centre for Medium-Range Weather Forecasts ECMWF, Reading RG2 9AX, UK. [7]Cooperative Institute for Research in Environmental Sciences, University of Colorado, Boulder, Colorado 80309, USA. [8]Physical Sciences Division, Earth System Research Laboratory, National Oceanic and Atmospheric Administration, Boulder, Colorado 80305, USA. *e-mail: stefan.broennimann@giub.unibe.ch

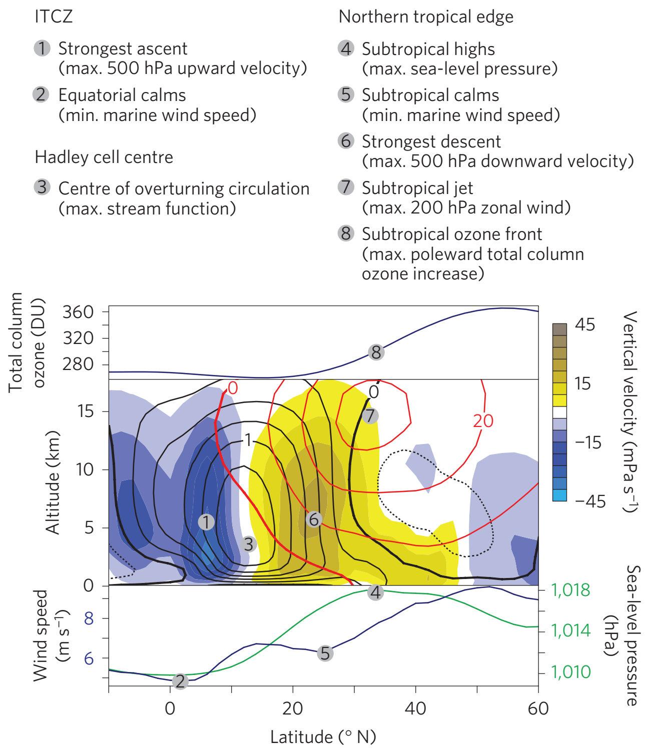

Figure 1 | Schematic diagram of the tropical edge and measures of its position. Contours show the 1945–1980 climatology of the zonal mean zonal wind (red, m s^{-1}) and the zonal mean meridional stream function (black, 10^9 kg s^{-1}) in boreal winter from the 20CR reanalysis v2c. The shading represents the climatological vertical velocity (mPa s^{-1}). The top and bottom panels show zonal mean total column ozone, sea-level pressure (both from 20CR v2c) and marine 10 m wind speed (ERA-20C).

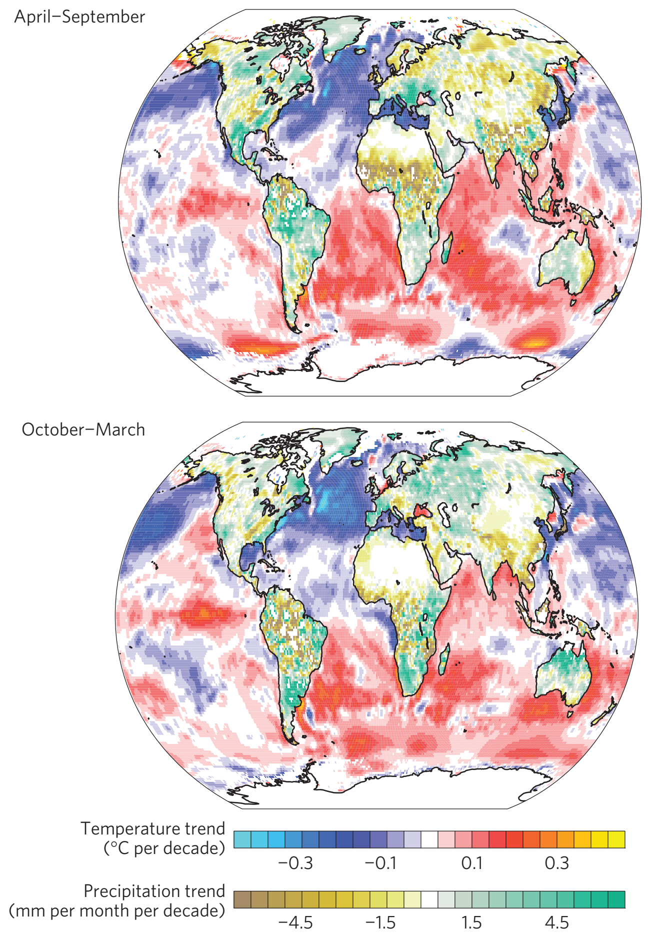

Figure 2 | Trends in sea-surface temperature and land precipitation from observations, 1945–1980. Trends were calculated with least-squares regression from seasonal averages of sea-surface temperature[24] (HadISST1.1) and precipitation (GPCC reanalysis Version 6; ref. 40). Boreal summer precipitation trends are significant over the Sahel region and southeastern Europe, sea-surface temperature trends are significant over most of the Atlantic, Indian and Southern oceans (see Supplementary Fig. 1 for trend significance).

fields based on surface and upper-air observations (here termed REC1 (ref. 18) and REC2 (ref. 19)) and a reconstruction of atmospheric ozone based on assimilating ground-based and satellite total column ozone observations into chemistry–climate model simulations (HISTOZ; ref. 20) are available. In total, eight global data sets are used in our study (note that REC2 is spatially incomplete), some of which are largely or even fully independent, thus providing a more comprehensive view than one data set alone.

Here we use the reanalysis data sets to calculate trends in latitude–height cross-sections of the zonal mean zonal wind $\overline{u}$ and the zonal mean meridional stream function ψ for different seasons using least-squares regression. Trends in ψ in 20CR v2c (Fig. 3) show a dipole-like structure, with an increase (decrease) on the southern (northern) side of the maximum in both seasons, more pronounced in winter. Similar results are also found for 20CR v2 and ERA-20C (Supplementary Fig. 2). The dipole structure implies a southward shift of the northern Hadley cell. This is illustrated by contrasting contours of $\overline{u}$ and ψ representative for the years 1945 and 1980 as obtained with the linear trend fit. The red contours (representing 1980) of ψ lie mostly equatorward of the black contours (representing 1945) by one or even several degrees latitude. For $\overline{u}$, a similar result is found for the winter season. A dipole trend pattern appears, with a strengthening to the south and a weakening to the north of the jet maximum, implying an equatorward shift. In summer the main trend is a weakening of the jet with little displacement.

Southward shift in observations and model

To further address latitudinal trends in atmospheric circulation features, we used the above-mentioned data sets (except ICOADS winds) in the form of monthly zonal averages to calculate indices of the tropical belt width and position (Methods and Supplementary Table 2). Our indices (indicated schematically in Fig. 1) capture the positions of the subtropical calms over the oceans (in ERA-20C, which is the only data set we use that ingests observed surface marine winds), the subtropical highs (HadSLP, all reanalyses), the strongest descent at 500 hPa (all reanalyses), the subtropical jet (maximum of $\overline{u}$ at 200 hPa, from REC1, REC2 and all reanalyses) and of the maximum meridional gradient of total column ozone (HISTOZ and all reanalyses). Furthermore, we also analysed the positions of the Hadley cell centre (maximum of ψ in all reanalyses) and of the ITCZ (maximum ascent at 500 hPa in all reanalyses as well as equatorial calms over the ocean in ERA-20C). The monthly indices were then averaged into boreal summer (April to September) and winter (October to March) seasons and series of the same index from different data sets were averaged.

The data sets and measures should be assessed critically. The indices stem from different data sources and measure different aspects of tropical and subtropical circulations (Fig. 1). However, most indices are significantly correlated on an interannual scale, including those of the ITCZ position and of the tropical edge position. The subtropical high index is well correlated with other edge indices only in winter, but not in summer, while the subtropical

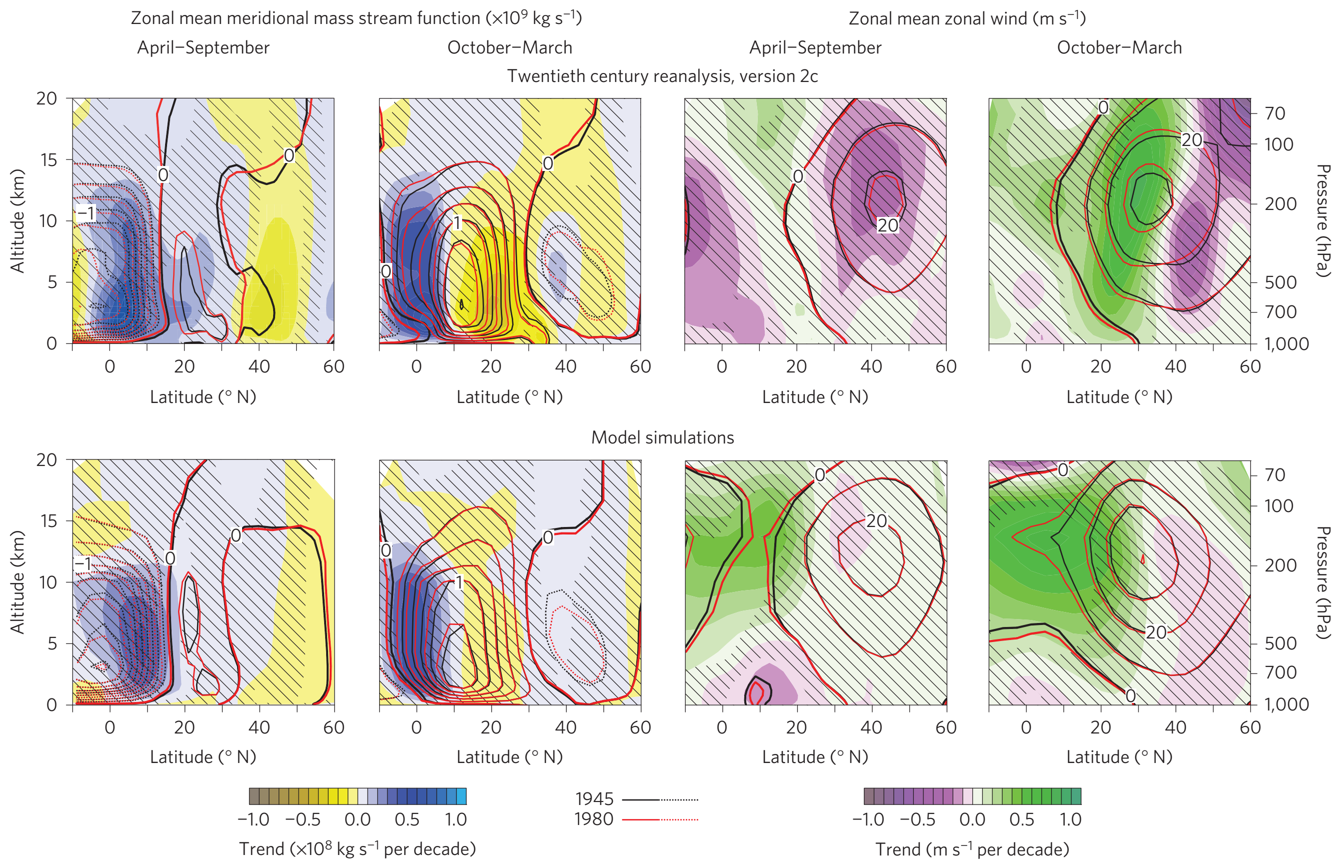

Figure 3 | Latitude–height cross-section of trends in the zonal and meridional circulation, 1945–1980. Contours show the trend fit of the zonal mean meridional mass stream function (left) and the zonal mean zonal wind (right) in boreal summer and winter for the years 1945 (black) and 1980 (red). Shading shows trends over the 1945–1980 period (hatching means not significant at $p < 0.05$). The top row is based on 20CR v2c and the bottom row on the ensemble mean of the SOCOL 'all forcings' simulations.

calms and total ozone indices are well correlated with other indices in summer, but not in winter (Supplementary Table 1). The indices also exhibit similar long-term behaviour (Fig. 4). Their trends confirm that the ITCZ moved southwards in both seasons. This is in agreement with previous studies[8,9,21], which found a southward shift of the tropical rain belt and the ITCZ during the second half of the twentieth century. Our study shows that this southward shift of the ITCZ coincided with a similar southward shift of the Hadley Cell centre and of the northern tropical edge that was not previously reported. This points to a picture of wider reorganization of the Hadley circulation that links historical shifts from drought to non-drought conditions in south central Europe with shifts from non-drought to drought conditions in the Sahel.

All 16 calculated index trends are negative. According to a binomial test (accounting for the effective degrees of freedom N^* in the series[22]) the p-values for all trends having the same sign is $p = 0.0045$. Moreover, nine trends are statistically significant on a 95% confidence level (Fig. 4). Thus, the individual metrics and the overall picture clearly support a southward shift of the tropical belt. Depending on the index series, the best estimate for the shift amounts to 0.25–1.5° latitude over the period. The results reinforce the hypotheses of Lamb[10] and Allen *et al.*[11], which can now be supported by various independent data sets.

These results are further confirmed by historical observations of surface marine winds (Supplementary Fig. 3) and corresponding ERA-20C reanalysis data, which allow tracing the northern and southern edges of the Hadley cell as regions with near-zero zonal and meridional winds, respectively (Methods). Between 1945–1954 and 1971–1980 (Supplementary Fig. 3) the ITCZ moved southwards in both seasons and basins. The northern edge moved southwards in both seasons in the Pacific, whereas observations in the Atlantic region show a southward shift only in winter.

In the following, the observation-based results are compared with an initial-condition ensemble of nine simulations of the twentieth century with the chemistry–climate model SOCOL (ref. 23). The interactive chemistry allows an analysis of the tropical edge position in total column ozone. Simulations were performed in an 'all forcings' set-up (termed ALL), where sea-surface temperatures (SSTs) and sea ice[24], greenhouse gases, solar irradiance, stratospheric aerosols, and tropospheric trace gas emissions were prescribed in a transient manner, while tropospheric aerosols were prescribed according to a climatology[25]. All indices (except for the calms, as 10 m wind speeds were not available) were calculated in the same way as in observation-based data: separately for each ensemble member, and then averaged.

Trends in latitude–height sections in the ensemble mean of the model simulations (Fig. 3) exhibit a southward shift of the ITCZ that is similar to that in reanalyses (note, however, that both the model and reanalyses specify the evolution of SSTs). Trends near the northern edge are not (or only barely) significant ($p = 0.05$) in the model. A dipole-like trend pattern appears for the zonal mean zonal wind in boreal winter similar to all reanalyses. In boreal summer, the agreement is worse, and at the same time the differences between the reanalyses are larger (Supplementary Fig. 2).

Indices of the latitudinal position of circulation features provide a more detailed view of tropical belt shifts in the simulations. An overview of the corresponding trends in the observation-based and model-based indices is given in Fig. 5. In the model,

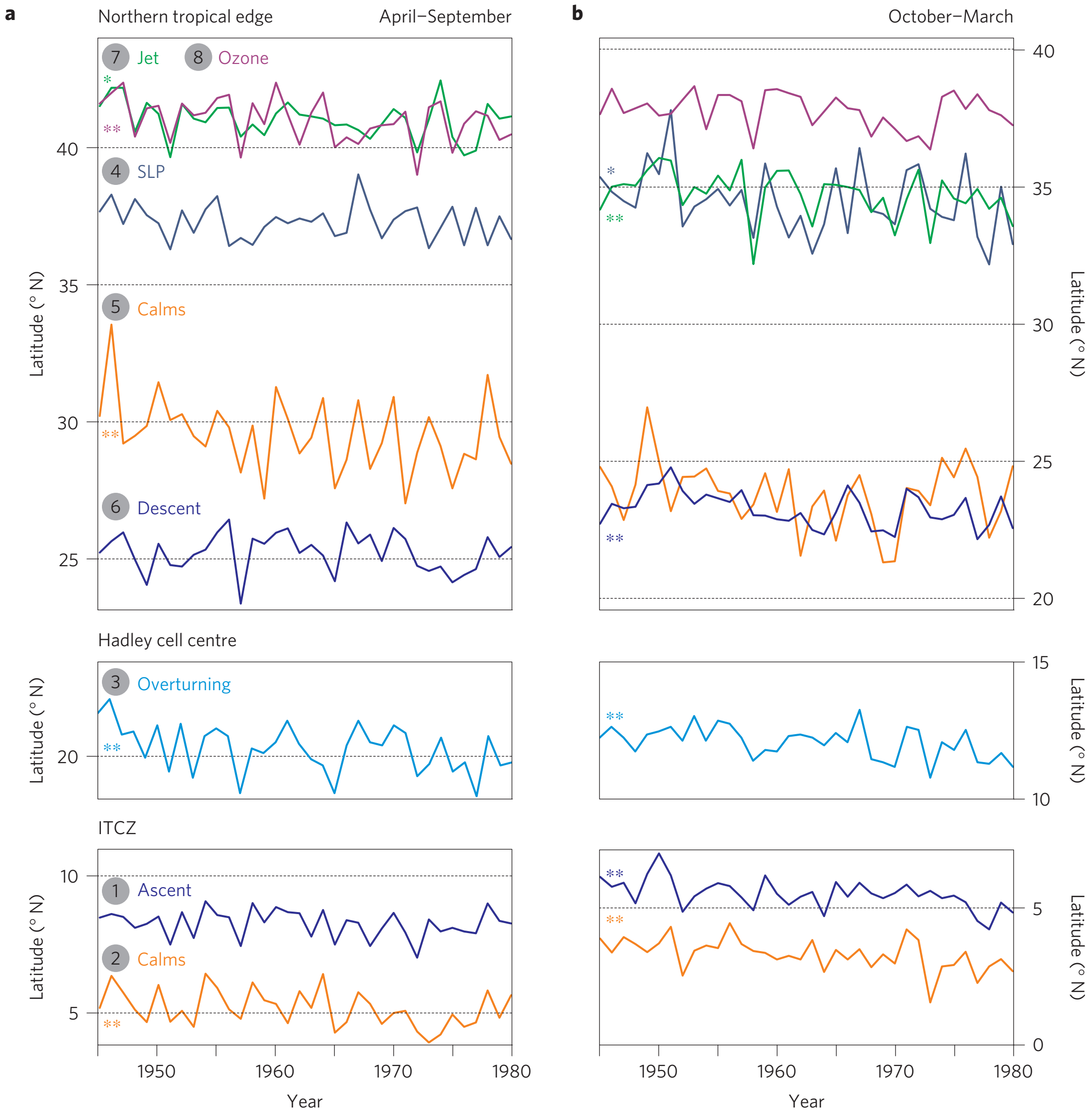

Figure 4 | Changes in the northern tropical belt. a,b, Time series of the latitude of the northern tropical edge (defined by the subtropical jet, the largest total column ozone meridional gradient, the maximum sea-level pressure, maximum descent and subtropical calms), the Hadley Cell centre (maximum meridional stream function) and the ITCZ (maximum 500 hPa upward velocity and equatorial calms) in April–September (**a**) and October–March (**b**). See Fig. 1 for an explanation of the indices. Trends in these series that are significant at the 90% and 95% confidence limits are marked with * and **, respectively.

11 out of 12 trends are negative (6 significant at the 95% confidence level). As for the observation-based indices, the overall picture of the negative trends in several circulation features provides evidence of an equatorward shift of the northern tropics in the model. Trends for northern tropical edge indices in summer are more variable in the model than in observation-based data. Also, the trends in the positions of descent (#6) and total column ozone increase (#8) are smaller in the model. All other trend magnitudes of model and observations are within each other's 95% confidence intervals. Model and observations are thus consistent. Studies on the recent widening found that atmospheric models forced with observed SSTs better capture the observed widening trend than coupled models, although they still strongly underestimate the trend magnitude[11,26].

An additional ensemble of three simulations was performed in which SSTs were prescribed from a climatology representative of 1900 conditions (Methods). To assess the effect of SSTs on the trend, we analysed the difference of the trends between the two ensembles (blue rectangles in Fig. 5). The ensemble with climatological SSTs but transient external forcings shows mostly small poleward shifts, and hence the trend difference is somewhat larger than trends in ALL. This implies that, in the model, the trends found in ALL can be explained entirely by SSTs (in the real world, the latter are of course not independent of the forcings).

Decadal oceanic variability or aerosols?

How did the SSTs change? The main feature of the trend over the 1945–1980 period is a cooling north of the Equator and a warming south of the Equator, particularly in the Atlantic (Fig. 2). This pattern can also be described as a negative trend in the Atlantic Multidecadal Oscillation (AMO). Strong interhemispheric gradients in temperature trends are understood to drive the latitudinal position of the ITCZ on decadal timescales[21], which is consistent with our findings. Specifically, the Sahel pluvial during the 1950s and subsequent droughts have been attributed to changes in the interhemispheric temperature gradient during these decades[8,27,28]. Moreover, it has been shown that summer temperature and precipitation over Southern Europe[29] and in the USA[30] are affected by the AMO, which reached a strongly positive phase during

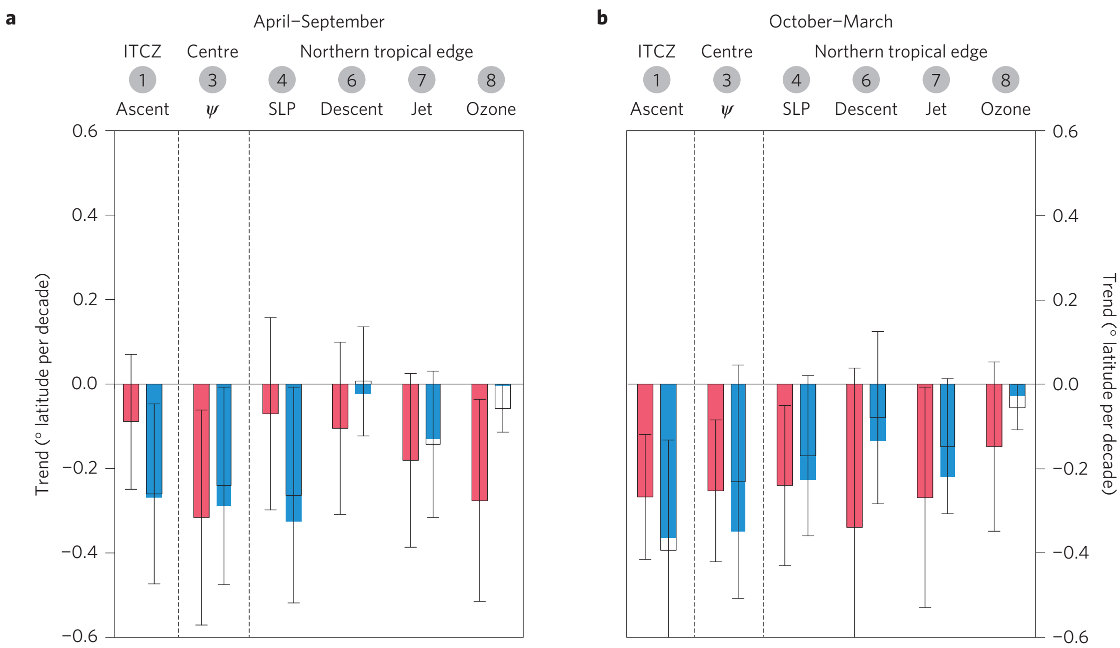

Figure 5 | Trends in the latitudinal position of the northern tropical belt in observation-based data and model simulations, 1945–1980. a,**b**, Trends are for the position of the ITCZ (maximum ascent), the Hadley cell centre and four indices for the northern tropical edge (see Fig. 1 for an explanation of the indices) in April to September (**a**) and October to March (**b**). The observation-based trends are shown as filled red bars, those of the 'all forcings' simulations as empty bars. Whiskers indicate 95% confidence intervals of the trend. The contribution of sea-surface temperature (blue boxes) indicates the difference in the trends between the 'all forcings' simulations and an ensemble of three simulations with sea-surface temperature held constant.

the late 1940s and early 1950s. Although the relation of droughts in these regions to the low-level moisture flux and the large-scale circulation is more complex than implied in Fig. 1, the associated circulation changes are part of the tropical edge shift. Changes in hydroclimate and the tropical belt position are thus consistent with specific SST trend patterns altering the atmospheric flow and precipitation patterns[31].

Various factors have been held responsible for the change in SSTs: internal variability of the North Atlantic Ocean[32] as well as forcing due to anthropogenic aerosols[33,34], which was specifically addressed in the context of Sahel drying and ITCZ shifts[35–37]. The low-frequency residual of El Niño Southern Oscillation also is expected to have played a role, particularly in the Pacific and Indian Oceans[38]. If future studies identify natural variability as the main cause, this implies that improvements in ocean initialization of decadal forecasts might help to better depict future changes in the tropical edge position. If aerosols are found to play the dominant role, this points to the importance of understanding future aerosol levels in projecting future changes of SSTs and the tropical belt.

Our results are consistent with a shift of the northern tropical belt of about 0.25° latitude per decade—that is, a shift of roughly 1° in latitude over the 1945 to 1980 period. Although this amounts to only around 100 km, shifts were arguably much larger regionally and were highly relevant in areas of strong precipitation gradients. Our findings indicate that interannual-to-multidecadal changes in the tropical belt due to changes in SSTs are an important component of climate variability. A southward shift from 1945 to 1980 also has implications for interpreting the current widening of the tropical belt, which might have started from a southward shifted state.

Data from the tropics and Southern Hemisphere are still sparse, but would allow a more complete view of changes in the Hadley circulation in this period. Current efforts[39] are small steps towards Lamb's grand vision: 'Knowledge of the great climatic changes of the past can help in the development of long-range weather forecasts. But the work of collecting, and putting into order, sufficient data on a worldwide scale is only just beginning'[10].

Methods

Methods and any associated references are available in the online version of the paper.

Received 6 July 2015; accepted 22 September 2015; published online 19 October 2015; corrected online 10 November 2015

References

1. Seidel, D. J., Fu, Q., Randel, W. J. & Reichler, T. J. Widening of the tropical belt in a changing climate. *Nature Geosci.* **1,** 21–24 (2008).
2. Davis, S. M. & Rosenlof, K. H. Multidiagnostic intercomparison of tropical-width time series using reanalyses and satellite observations. *J. Clim.* **25,** 1061–1078 (2012).
3. Hudson, R. D. Measurements of the movement of the jet streams at mid-latitudes, in the Northern and Southern Hemispheres, 1979 to 2010. *Atmos. Chem. Phys.* **12,** 7797–7808 (2012).
4. Hartmann, D. L. *et al.* in *Climate Change 2013: The Physical Science Basis* (eds Stocker, T. F. *et al.*) 159–254 (IPCC, Cambridge Univ. Press, 2013).
5. Quan, X.-W., Hoerling, M. P., Perlwitz, J., Diaz, H. F. & Xu, T. How fast are the tropics expanding? *J. Clim.* **27,** 1999–2013 (2014).
6. Post, D. A. *et al.* Decrease in southeastern Australian water availability linked to ongoing Hadley cell expansion. *Earth's Future* **2,** 231–238 (2014).
7. Marengo, J. Variations and change in South American streamflow. *Climatic Change* **31,** 99–117 (1995).
8. Held, I. M., Delworth, T. L., Lu, J., Findell, K. L. & Knutson, T. R. Simulation of Sahel drought in the 20th and 21st centuries. *Proc. Natl Acad. Sci. USA* **102,** 17891–17896 (2005).
9. Hwang, Y.-T., Frierson, D. M. W. & Kang, S. M. Anthropogenic sulfate aerosol and the southward shift of tropical precipitation in the late 20th century. *Geophys. Res. Lett.* **40,** 2845–2850 (2013).
10. Lamb, H. H. The new look of climatology. *Nature* **23,** 1209–1215 (1969).
11. Allen, R. J., Norris, J. R. & Kovilakam, M. Influence of anthropogenic aerosols and the Pacific Decadal Oscillation on tropical belt width. *Nature Geosci.* **7,** 270–274 (2014).
12. Compo, G. P. *et al.* The Twentieth Century Reanalysis Project. *Q. J. R. Meteorol. Soc.* **137,** 1–28 (2011).
13. Lu, J., Deser, C. & Reichler, T. Cause of the widening of the tropical belt since 1958. *Geophys. Res. Lett.* **36,** L03803 (2009).
14. Birner, T. Recent widening of the tropical belt from global tropopause statistics: Sensitivities. *J. Geophys. Res.* **115,** D23109 (2012).

15. Allan, R. & Ansell, T. A new globally complete monthly historical gridded mean sea level pressure dataset (HadSLP2): 1850–2004. *J. Clim.* **19,** 5816–5842 (2006).
16. Woodruff, S. D. *et al.* ICOADS Release 2.5: Extensions and enhancements to the surface marine meteorological archive. *Int. J. Climatol.* **31,** 951–967 (2011).
17. Poli, P. *et al. ERA-20C Deterministic* ERA Report Series 20 (ECMWF, 2015).
18. Griesser, T. *et al.* Reconstruction of global monthly upper-level temperature and geopotential height fields back to 1880. *J. Clim.* **23,** 5590–5609 (2010).
19. Brönnimann, S., Griesser, T. & Stickler, A. A gridded monthly upper-air data set from 1918 to 1957. *Clim. Dynam.* **38,** 475–493 (2012).
20. Brönnimann, S. *et al.* A global historical ozone data set and prominent features of stratospheric variability prior to 1979. *Atmos. Chem. Phys.* **13,** 9623–9639 (2013).
21. Schneider, T., Bischoff, T. & Haug, G. H. Migrations and dynamics of the intertropical convergence zone. *Nature* **513,** 45–53 (2014).
22. Bretherton, C. S., Widmann, M., Dymnikov, V. P., Wallace, J. M. & Bladé, I. The effective number of spatial degrees of freedom of a time-varying field. *J. Clim.* **12,** 1990–2009 (1999).
23. Schraner, M. *et al.* Technical note: Chemistry–climate model SOCOL: Version 2.0 with improved transport and chemistry/microphysics schemes. *Atmos. Chem. Phys.* **8,** 5957–5974 (2008).
24. Rayner, N. A. *et al.* Global analyses of SST, sea ice and night marine air temperature since the late nineteenth century. *J. Geophys. Res.* **108,** 4407 (2003).
25. Fischer, A. M. *et al.* Interannual-to-decadal variability of the stratosphere during the 20th century: Ensemble simulations with a chemistry–climate model. *Atmos. Chem. Phys.* **8,** 7755–7777 (2008).
26. Allen, R. J., Sherwood, S. C., Norris, J. R. & Zender, C. S. Recent Northern Hemisphere tropical expansion primarily driven by black carbon and tropospheric ozone. *Nature* **485,** 350–355 (2012).
27. Biasutti, M., Held, I. M., Sobel, A. H. & Giannini, A. SST forcings and Sahel rainfall variability in simulations of the 20th and 21st centuries. *J. Clim.* **21,** 3471–3486 (2008).
28. Martin, E. R., Thorncroft, C. & Booth, B. B. B. The multidecadal Atlantic SST—Sahel rainfall teleconnection in CMIP5 simulations. *J. Clim.* **27,** 784–806 (2014).
29. Sutton, R. T. & Dong, B. Atlantic Ocean influence on a shift in European climate in the 1990s. *Nature Geosci.* **5,** 788–792 (2012).
30. Nigam, S., Guan, B. & Ruiz-Barradas, A. Key role of the Atlantic Multidecadal Oscillation in 20th century drought and wet periods over the Great Plains. *Geophys. Res. Lett.* **38,** L16713 (2011).
31. Mohino, E., Janicot, S. & Bader, J. Sahel rainfall and decadal to multi-decadal sea surface temperature variability. *Clim. Dynam.* **37,** 419–440 (2011).
32. Knight, J. R., Folland, C. K. & Scaife, A. A. Climate impacts of the Atlantic Multidecadal Oscillation. *Geophys. Res. Lett.* **33,** L17706 (2006).
33. Booth, B. B. B., Dunstone, N. J., Halloran, P. R., Andrews, T. & Bellouin, N. Aerosols implicated as a prime driver of twentieth-century North Atlantic climate variability. *Nature* **484,** 228–232 (2012).
34. Zhang, R. *et al.* Have aerosols caused the observed Atlantic multidecadal variability? *J. Atmos. Sci.* **70,** 1135–1144 (2013).
35. Kawase, H. *et al.* Physical mechanism of long-term drying trend over tropical North Africa. *Geophys. Res. Lett.* **37,** L09706 (2010).
36. Ackerley, D. *et al.* Sensitivity of twentieth-century Sahel rainfall to sulfate aerosol and CO_2 forcing. *J. Clim.* **24,** 4999–5014 (2011).
37. Ridley, H. E. *et al.* Aerosol forcing of the position of the intertropical convergence zone since AD 1550. *Nature Geosci.* **8,** 195–200 (2015).
38. Compo, G. P. & Sardeshmukh, P. D. Removing ENSO-related variations from the climate record. *J. Clim.* **8,** 1957–1978 (2010).
39. Allan, R. *et al.* The International Atmospheric Circulation Reconstructions over the Earth (ACRE) initiative. *Bull. Am. Meteorol. Soc.* **92,** 1421–1425 (2011).
40. Schneider, U. *et al.* GPCC's new land surface precipitation climatology based on quality-controlled *in situ* data and its role in quantifying the global water cycle. *Theor. Appl. Climatol.* **115,** 15–40 (2014).

Acknowledgements

The authors wish to acknowledge support by the Swiss National Science Foundation (projects EVALUATE (130407) and FUPSOL-II (147659)), EU FP7 project ERA-CLIM2 (607029) and ERC Grant TITAN (320691). Support for the Twentieth Century Reanalysis Project data set is provided by the US Department of Energy, Office of Science Innovative and Novel Computational Impact on Theory and Experiment (DOE INCITE) programme, and Office of Biological and Environmental Research (BER), and by the National Oceanic and Atmospheric Administration Climate Program Office. We wish to thank all data providers.

Author contributions

S.B. designed the study, conducted most analyses and prepared the manuscript. A.M.F. and E.R. performed the model simulations. P.P. provided data sets and conducted wind analyses. G.P.C. and P.D.S. provided data sets and suggested some of the analyses. All authors assisted in the interpretation of the data, discussed results and commented on the manuscript.

Additional information

Supplementary information is available in the online version of the paper. Reprints and permissions information is available online at www.nature.com/reprints. Correspondence and requests for materials should be addressed to S.B.

Competing financial interests

The authors declare no competing financial interests.

Methods

Data. REC1 (ref. 18) is a reconstruction of monthly hemispheric (15°–90° N) upper-level geopotential height and temperature fields from historical upper-level and surface data. It is based on principal component regression using ERA-40 (ref. 41) as a target and is spatially complete, but assumes stationarity of hemispheric principal component patterns. REC1 is complemented with ERA-40 after 1957. REC2 (ref. 19) is also a statistical reconstruction of monthly upper-level geopotential height, wind and temperature from historical upper-level and surface data. It also uses principal component regression and is calibrated using ERA-40. However, REC2 is a grid-column-by-grid-column reconstruction considering only predictors from a cone of influence around that grid column and requiring a minimum amount of upper-level observations. Thus, no stationarity of spatial patterns is assumed, but grid columns away from upper-air observations have no data. We took into account only grid cells that have a complete record from April 1943 onwards (no gap allowed). The spatial coverage is shown in Supplementary Fig. 1. This reduced data set was then zonally averaged for further processing. After 1957, REC2 was extended to 1980 using the reconstruction in the calibration period[19].

The data set HISTOZ is based on an assimilation of historical ground-based and satellite total column ozone observations into the ALL ensemble simulations with the SOCOL chemistry–climate model[20]. After 1979, HISTOZ is supplemented by the BDBP satellite-based ozone data set[42].

The spatial resolutions of the data sets differ. REC1 and REC2 have a resolution of 2.5° in longitude and latitude, 20CR has a 2° resolution, HISTOZ and HadSLP are coarser, with a resolution of 5° . SOCOL has a resolution of 3.8°. To keep the resolutions of the data sets similar, we used ERA-20C in a 2° × 2° resolution for calculating the indices. For further analyses we also used ICOADS wind data[16] as well as the global GPCC precipitation data[40].

Note that HISTOZ is entirely independent of REC1, REC2 and HadSLP. HISTOZ, REC1 and REC2 are quasi-independent of the reanalyses. HISTOZ shares with the reanalyses the dependence on model boundary conditions (including SSTs), but the increments in the Northern Hemisphere subtropics are substantial and HISTOZ differs significantly from the background[20]. REC1, REC2 and the reanalyses share sea-level pressure information, but the weight of this is strongly limited in the reconstructions.

The marine surface winds from ICOADS (ref. 16) provide historical observational records of atmospheric circulation covering many regions of the globe over the time period of interest (years 1945 to 1980). A proxy for the edges of the Hadley cell is to observe where the wind changes direction—that is, where one of its components crosses zero. Such a signal is more robust for the wind component shifting between two strong regimes, and over oceans, as orography affects wind over land. In Supplementary Fig. 3 we show near-zero contours for average zonal and meridional wind.

Indices. All indices were calculated from zonal averages of monthly fields. They are defined as the interpolated latitude φ of the minimum or maximum (here $\varphi_{\min}$) in a variable x within a given range. Definitions based on maxima or minima are preferred over zero-crossing positions, which may be affected more strongly by biases.

The interpolation (here for $\varphi_{\min}$) was obtained by:

$$\varphi_{\min} = \varphi_0 - \Delta\varphi \frac{x_1 - x_{-1}}{2|x_0 - \max(x_{-1}, x_1)|}$$

where subscripts 0, −1 and 1 refer to the value or latitude of the minimum (or maximum) x and its neighbours, $\Delta\varphi$ is the resolution.

Several of the analysed fields exhibit double maxima or minima not only in individual months, but even in the climatology (for example, vertical velocity as shown in Fig. 1). Therefore, it is important to restrict the accepted range as carefully as possible depending on the season (see Supplementary Table 2, note that due to the different resolution of SOCOL, slightly different ranges were used in that data set). If no local minimum (maximum) was found within the range, the corresponding edge of the range was chosen. If, in rare cases, more than one local minimum (maximum) was found, the more equatorward one (which could include a global minimum at the equatorward edge) was chosen for indices of the tropical edge but the global minimum was chosen for the ITCZ indices. The following indices were used (see Fig. 1):

Intertropical convergence zone (*ITCZ*). (1) Strongest ascent: Maximum upward vertical velocity ω at 500 hPa in the tropics from 20CR v2, 20CR v2c, ERA-20C and SOCOL. Restricting the accepted range reduces ambiguities. (2) Equatorial calms: Latitude of lowest 10 m wind speed over the oceans near the Equator in ERA-20C.

Hadley cell centre. (3) Centre of meridional overturning: The latitude of the maximum of ψ in the northern tropics at any level between 500 hPa and 700 hPa in 20CR v2, 20CR v2c, ERA-20C and SOCOL. Occasionally, the maximum occurs at an even lower level, but in these cases there was often an ambiguity, which can be avoided by restricting the lowest level to 700 hPa.

Northern tropical edge. (4) Subtropical highs: The latitude of the maximum sea-level pressure in the subtropics in HadSLP, 20CR v2, 20CR v2c, ERA-20C, and SOCOL. (5) Subtropical calms: Latitude of lowest 10 m wind speed over the oceans in the subtropics in ERA-20C. (6) Strongest descent: Latitude of the maximum downward vertical velocity ω at 500 hPa in the subtropics in 20CR v2, 20CR v2c, ERA-20C and SOCOL. At that level, ambiguities can be avoided. (7) Subtropical jet: Latitude of the maximum of $\overline{u}$ at 200 hPa in the subtropics in 20CR v2, 20CR v2c, ERA-20C, REC1, REC2 and SOCOL. For REC1 we used the latitudinal gradient in zonally averaged 200 hPa geopotential height. The 200 hPa level was chosen because those instances in which the wind maximum was not at 200 hPa were rare. (8) Subtropical ozone front: Maximum meridional total column ozone gradient in the subtropics in HISTOZ, 20CR v2, 20CR v2c, ERA-20C and SOCOL.

The monthly indices and fields were then averaged into boreal summer (April to September) and winter (October to March) seasons. Further, we averaged the series from all different data sets.

Model. The SOCOL model[23] and the set-up of the ALL simulations[25] are described in detail in the literature. Simulations with fixed SSTs were performed starting in 1901 and using a climatology derived from observed[24] SSTs from 1886 to 1915. SSTs for these years were averaged after excluding the volcanically perturbed years (that is, two years after the eruption of St. Maria in October 1902 and two years after the eruption of Mt. Katmai in June 1912). Furthermore, strong ENSO events in the 30-yr period were removed before averaging according to Table 1 in Brönnimann and colleagues[43].

Data sources. 20CR and 20CR v2c can be downloaded from http://www.esrl.noaa.gov/psd/data/20thC_Rean

ERA-20C can be downloaded from http://apps.ecmwf.int/datasets/data/era20c-daily

REC1 and REC2 are available from the Bern Open Repository (BORIS) at http://boris.unibe.ch/id/eprint/71204 with further information and details from http://www.oeschger.unibe.ch/research/databases/CHUAN

HISTOZ is available from the Bern Open Repository (BORIS) at http://boris.unibe.ch/id/eprint/71600

ICOADS can be downloaded from http://rda.ucar.edu/datasets/ds540.0

HadISST1.1 can be downloaded from http://www.metoffice.gov.uk/hadobs/hadisst

GPCC can be downloaded from http://www.esrl.noaa.gov/psd/data/gridded/data.gpcc.html

SOCOL simulations are available from the Bern Open Repository (BORIS) at http://boris.unibe.ch/id/eprint/71204

Code availability. The R code used to calculate the indices is available from the Bern Open Repository (BORIS) at http://boris.unibe.ch/id/eprint/71204

For simple operations (such as interpolation, masking, extraction, averaging) and standard statistics (linear least-squares regression, correlation, calculation of degrees of freedom) standard packages of R were used.

References

41. Uppala, S. M. *et al.* The ERA-40 reanalysis. *Q. J. R. Meteorol. Soc.* **131,** 2961–3012 (2005).
42. Bodeker, G. E., Hassler, B., Young, P. J. & Portmann, R. W. A vertically resolved, global, gap-free ozone database for assessing or constraining global climate model simulations. *Earth Syst. Sci. Data* **5,** 31–43 (2013).
43. Brönnimann, S., Xoplaki, E., Casty, C., Pauling, A. & Luterbacher, J. ENSO influence on Europe during the last centuries. *Clim. Dynam.* **28,** 181–197 (2007).

Erratum: Southward shift of the northern tropical belt from 1945 to 1980

Stefan Brönnimann, Andreas M. Fischer, Eugene Rozanov, Paul Poli, Gilbert P. Compo and Prashant D. Sardeshmukh

Nature Geoscience http://dx.doi.org/10.1038/ngeo2568 (2015); published online 19 October 2015; corrected online 10 November 2015.

In the version of this Letter originally published online, the titles of the *x* axes in Figures 1 and 3 were incorrect; they should have read 'Latitude (° N)'. This is now correct in all versions of the Letter.